WIRELESS COMMUNICATIONS AND MOBILE COMPUTING
Wirel. Commun. Mob. Comput. 2004; **4**:711–725
Published online in Wiley InterScience (www.interscience.wiley.com). DOI: 10.1002/wcm.250

Improving the performance of coded FDFR multi-antenna systems with turbo-decoding‡

Renqiu Wang[1], Xiaoli Ma[2] and Georgios B. Giannakis[1]*,†

[1]*Department of Electrical and Computer Engineering, University of Minnesota, 200 Union Street SE, Minneapolis, MN 55455, U.S.A.*
[2]*Department of Electrical and Computer Engineering, Auburn University, Auburn AL 36849, U.S.A.*

Summary

A full-diversity full-rate (FDFR) multi-antenna system was developed recently, enabling uncoded layered space-time (LST) transmissions to achieve full-diversity (N_tN_r) and full-rate (N_t symbols per channel use) simultaneously, for any number of transmit antennas N_t and receive antennas N_r. In this paper, we investigate the performance of a coded FDFR design obtained by concatenating an error control coding (ECC) module and FDFR module with a random interleaver in between. Turbo decoding is performed at the receiver. With R_c denoting the ECC rate, d_{min} the minimum Hamming distance of the ECC, and M the constellation size, an overall transfer rate of $R_cN_t\log_2 M$ bits per channel use and a full diversity order $d_{min}N_tN_r$ are achieved. Different ECC choices are considered. Approximate analysis reveals that multi-stream ECC and single-stream ECC make no difference when convolutional codes with long frame length and near-optimal MIMO decoding schemes are adopted. Without sacrificing rate, the coded FDFR system improves error performance compared with coded V-BLAST, when relatively weak codes are used. As N_r increases, even strong codes such as rate 1/2 turbo codes can benefit from FDFR. Specifically, 1.5–2 dB gain over coded V-BLAST is obtained in a 2×2 antenna setup when convolutional codes or rate 3/4 turbo codes are used; 0.5 dB gain is offered in a 2×5 setup when rate 1/2 turbo codes are used. Coded FDFR also outperforms a 16-QAM Alamouti coded scheme by 1 dB when convolutional codes are used. The price paid is increased complexity. Copyright © 2004 John Wiley & Sons, Ltd.

KEY WORDS: space-time; diversity; V-BLAST; FDFR; turbo decoding

1. Introduction

High transmission rate and low error rate are the ultimate goals of modern wireless communication modems, which are challenged by multiplicative channel fading and additive Gaussian noise (AGN) effects. Traditional error control coding (ECC) over the Galois field (GF) deals with AGN and fading by adding redundancy. Allowing for long block or large interleaver sizes, thus assuming unconstrained encoding and decoding complexity, low-density parity check (LDPC) codes and turbo codes approach the

*Correspondence to: Georgios B. Giannakis, Department of Electrical and Computer Engineering, University of Minnesota, 200 Union Street SE, Minneapolis, MN 55455, U.S.A.
†E-mail: georgios@ece.umn.edu
‡Part of the results in this paper was presented at *IEEE International Symposium on Signal Processing and Information Technology* December 14–17, 2003, Darmstadt, Germany. Guest Editor: Dr. E.G. Larsson, email: egl@gwu.edu

Contract/grant sponsors: ARL/CTA; contract/grant number: DAAD 19-01-2-0011.

bit error rate (BER) limit dictated by channel capacity [1–3]. However, when delay or complexity is constrained, alternative low-complexity ECC options become more practical, among which convolutional codes (CC) are often preferable due to their simple yet flexible structure and mature low-complexity Viterbi decoding [4]. Although ECC is a well-documented means of improving error performance, it reduces spectral efficiency due to the redundancy inserted. Bandwidth-efficient means of mitigating channel fading by exploiting diversity flavors in other dimensions are thus well motivated. Linear complex field (LCF) coding and space-time (ST) coding are two such flavors, in the precoded modulation and spatial dimensions respectively. LCF coding (LCFC) is the counterpart of GF coding. With each entry of the generator matrix chosen from the complex field, LCFC has been shown capable of enabling maximum diversity with small or no rate loss; see for example References [5–9] and references thereof. The principle is to construct a $P \times P$ encoder matrix which produces codewords with any pairwise Hamming distance equal to P. Relying on multiple (N_t) transmit and multiple (N_r) receive antennas, multi-input multi-output (MIMO) spatial wireless links are created. It has been shown that the MIMO capacity of independent Rayleigh fading ergodic channels increases approximately linearly with the minimum of (N_t, N_r), implying that MIMO can potentially boost both diversity and data rate [10]. There have been many advances in this field, which in general fall into two classes: the first class aims at improving error performance by exploiting spatial diversity, while the second one targets high data rate. ST orthogonal designs [11,12] and ST trellis codes [13] are two examples in the first class. BLAST-type ST codes [14,15] and linear dispersion (LD) codes [16] belong to the second class.

Although, it is still worthwhile to fully explore the potential of each ST code design, jointly exploiting merits from two or more designs often leads to more desirable tradeoffs in rate-diversity-complexity. By concatenating an LCF coder with a layered ST (LST) mapper properly, the recently developed full-diversity full rate (FDFR) design [17] enables an uncoded LST system to have full diversity (N_tN_r) and full-rate (N_t symbols per channel use) simultaneously (see also Ref. [18]). Joint consideration of ECC and LCFC in ST setups was pursued also in Reference [19]. Although the triangular ST mapper developed in Reference [19] enables full diversity order $d_{\min}N_tN_r$, where $d_{\min}$ is the minimum Hamming distance or free distance of the ECC, the overall transmission rate is only about half of the maximum possible.

The performance of uncoded FDFR and Reference [19] motivate us to investigate the performance of a joint ECC and FDFR system in this paper. We will particularly consider relatively 'weakly' coded FDFR architectures, which rely on the concatenation of ECC, LCFC and ST multiplexing at the transmitter, along with soft-to-hard sphere decoding (SHD-SD) [20,21] with iterative detection at the receiver. After developing the system model in Section 2, we will analyze the diversity order of coded FDFR under the assumptions of near-perfect interleaving and near-optimal decoding. A few special cases, including CC and turbo coding (TC), will be considered in choosing a single-stream coding structure over its multi-stream counterpart. We will use coded V-BLAST as a reference in our performance comparisons. In Section 4, we will illustrate by simulations that the FDFR design offers notable performance improvement by enabling full spatial diversity without sacrificing rate, when CC or high rate TC is used, at the expense of increased complexity.

Notation: Upper (lower) bold face letters will be used for matrices (column vectors). Superscript * will denote Hermitian transpose and ^{T} indicates transpose. We will use $\otimes$ to stand for the Kronecker product; diag($\mathbf{v}$) will stand for a diagonal matrix with entries of the vector $\mathbf{v}$ on its main diagonal.

2. System Model

As depicted in Figure 1, the coded FDFR system concatenates an ECC module and an FDFR module with a random interleaver in between. Soft turbo decoding between the ECC decoding module and the FDFR decoding module is performed at the receiver end. Both MIMO channels and the FDFR code are decoded at the same time. We will use the term 'FDFR block' to denote an FDFR processing unit, 'ECC stream' for an ECC encoder unit, and 'frame' for a set of information bits that will be processed by the ECC module, the interleaver, and the FDFR module serially without dependence on another frame. We can also think of a frame as the system's processing unit.

2.1. The Transmitter and Equivalent MIMO Channels

A frame of information bits $\mathbf{b}$ with length K_c is first encoded by an ECC module to yield $\mathbf{c}$, and then goes

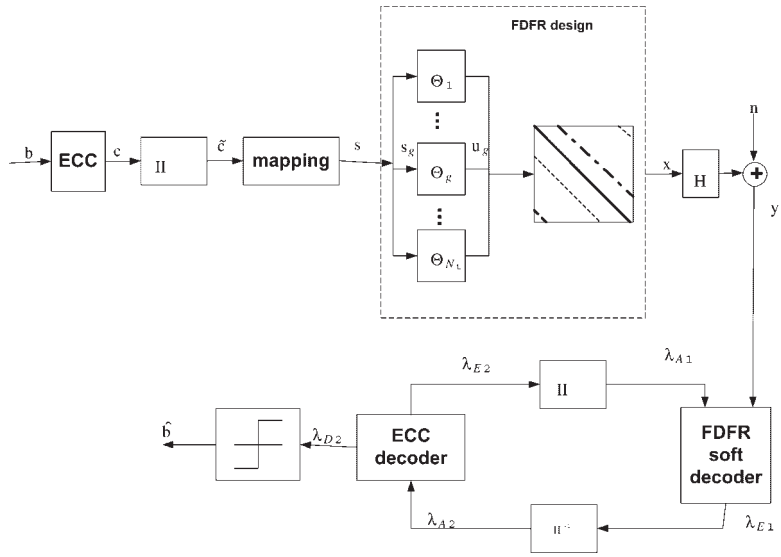

Fig. 1. The coded full-diversity full-rate (FDFR) system model.

through a random interleaver $\mathbf{\Pi}$. The ECC module with interleaver can implement either a single-stream coding structure as depicted in Figure 2, where information bits are processed serially by a single encoder, or, they can implement a multi-stream coding structure as depicted in Figure 3(a), where information bits are divided into n sub-streams and each sub-stream is encoded independently. As a special case of the multi-stream structure, the multi-steam per layer transmission is depicted in Figure 3(b), where instead of using one interleaver, the coded bits per sub-stream are scrambled with a sub-interleaver matrix $\mathbf{\Pi}_i$ independently. In this case, the equivalent overall interleaver matrix $\mathbf{\Pi}^{\mathrm{o}} = \mathrm{diag}([\mathbf{\Pi}_1 \ldots \mathbf{\Pi}_n])$ is no longer a random interleaver although each sub-interleaver $\mathbf{\Pi}_i$ can be random.

Interleaved bits $\tilde{\mathbf{c}}$ are mapped to a frame of symbols $\mathbf{f}$ with frame length N_c adhering to a certain constellation; $\mathbf{f}$ is then fed to the FDFR module. Frame $\mathbf{f}$ is divided first into FDFR blocks $\{\mathbf{s}(k)\}_{k=1}^{K}$ with block length N_{t}^2 symbols, where k indexes the FDFR block, and K is the number of blocks. Let us temporarily omit the block index k to explain the FDFR design. We will come back to it in Section 3. Each FDFR block $\mathbf{s}$ is then divided into N_{t} sub-blocks with sub-block length equal to N_{t}. Let $\mathbf{s}_g$ denote the gth $N_{\mathrm{t}} \times 1$ sub-block ($g = 1, \ldots, N_{\mathrm{t}}$), whose entries $\{s_{g,k}\}_{k=1}^{N_{\mathrm{t}}}$ are drawn from a complex finite alphabet set $\mathcal{S}$. The sub-block $\mathbf{s}_g$ is first coded to obtain

$$\mathbf{u}_g = \mathbf{\Theta}_g \mathbf{s}_g, \quad g = 1, \ldots, N_{\mathrm{t}} \tag{1}$$

where $\{\mathbf{\Theta}_g := \beta^{g-1}\mathbf{\Theta}\}_{g=1}^{N_{\mathrm{t}}}$ is the set of LCF encoders, β is a scalar and $\mathbf{\Theta}$ is chosen from the class of unitary Vandermonde matrices:

$$\mathbf{\Theta} = \frac{1}{\sqrt{N_{\mathrm{t}}}} \mathbf{F}_{N_{\mathrm{t}}}^{*} \mathrm{diag}[1, \alpha, \ldots, \alpha^{N_{\mathrm{t}}-1}] \tag{2}$$

where $\mathbf{F}_{N_{\mathrm{t}}}$ is the $N_{\mathrm{t}} \times N_{\mathrm{t}}$ FFT matrix with $(m+1, n+1)$st entry $e^{-j2\pi mn/N_{\mathrm{t}}}$, and α is a scalar. Three design approaches for β and $\mathbf{\Theta}$ (or equivalently α) have been derived to enable full-diversity and full-rate in Reference [17]. As an example, when $N_{\mathrm{t}} = 2^k$, with k being a natural number, design A selects $\alpha = e^{j\pi/(2N_{\mathrm{t}})}$ and $\beta^{N_{\mathrm{t}}} = e^{j\pi/(4N_{\mathrm{t}}^2)}$; design B selects $\alpha = e^{j\pi/N_{\mathrm{t}}^3}$ and $\beta^{N_{\mathrm{t}}} = \alpha$; and design C selects $\alpha = e^{j/2}$ and $\beta^{N_{\mathrm{t}}} = \alpha$ or α as in the design A, but with $\beta^{N_{\mathrm{t}}} = e^{j/2}$.

The LCF coded symbols $\{\mathbf{u}_g\}_{g=1}^{N_{\mathrm{t}}}$ then go through an LST mapper, and are transmitted through N_{t} antennas as follows:

$$\mathbf{V} = \begin{bmatrix} u_{1,1} & u_{N_{\mathrm{t}},2} & \ldots & u_{2,N_{\mathrm{t}}} \\ u_{2,1} & u_{1,2} & \ldots & u_{3,N_{\mathrm{t}}} \\ \vdots & \vdots & \ldots & \vdots \\ u_{N_{\mathrm{t}},1} & u_{N_{\mathrm{t}}-1,2} & \ldots & u_{1,N_{\mathrm{t}}} \end{bmatrix} \begin{matrix} \rightarrow \text{time} \\ \downarrow \text{space} \end{matrix} \tag{3}$$

Fig. 2. The single-stream error control coding (ECC) model.

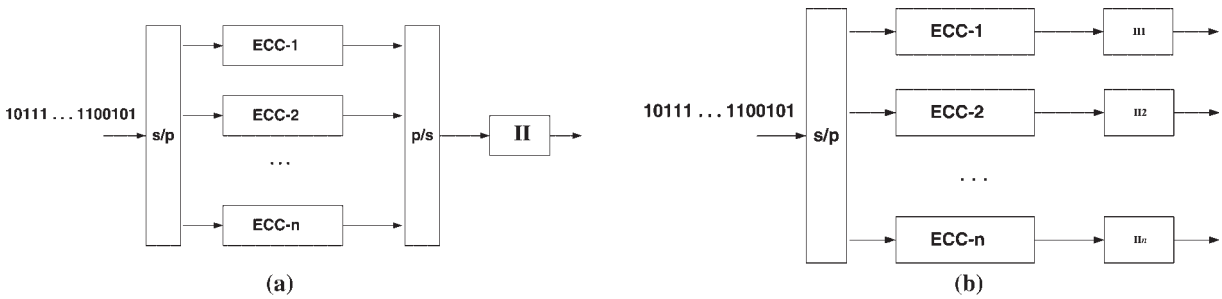

Fig. 3. (a) The multi-stream ECC model; (b) the multi-stream per layer model.

where $u_{g,i}$ denotes the ith entry of vector $\mathbf{u}_g$. Let $\mathbf{s} := [\mathbf{s}_1^T, \ldots, \mathbf{s}_{N_t}^T]^T$ denote one FDFR block and $\boldsymbol{\theta}_i^T$ denote the ith row of $\boldsymbol{\Theta}$. By defining the permutation matrix $\mathbf{P}_i$ and the diagonal matrix $\mathbf{D}_\beta$ respectively, as:

$$\mathbf{P}_i := \begin{bmatrix} \mathbf{0} & \mathbf{I}_{i-1} \\ \mathbf{I}_{N_t-i+1} & \mathbf{0} \end{bmatrix} \text{ and } \mathbf{D}_\beta := \text{diag}[1, \beta, \ldots, \beta^{N_t-1}]$$

we obtain the equivalent FDFR encoder for the entire block $\mathbf{s}$ as

$$\boldsymbol{\Phi} := \begin{bmatrix} (\mathbf{P}_1\mathbf{D}_\beta) \otimes \boldsymbol{\theta}_1^T \\ \vdots \\ (\mathbf{P}_{N_t}\mathbf{D}_\beta) \otimes \boldsymbol{\theta}_{N_t}^T \end{bmatrix} \tag{4}$$

and the FDFR output vector as $\mathbf{x} = \boldsymbol{\Phi}\mathbf{s}$.

We use $\mathbf{H}_l$ to denote the $N_r \times N_t$ MIMO channel coefficient matrix during the lth time slot that transmitted vector $\mathbf{V}_l$ is facing, where $\mathbf{v}_l$ denotes the lth column of matrix $\mathbf{v}$ given as in Equation (3). Thus, the channel matrix $\mathcal{H}$ for the transmitted vector $\mathbf{v} := [\mathbf{v}_1^T \ldots \mathbf{v}_{N_t}^T]^T$ can be written as:

$$\mathcal{H} := \begin{bmatrix} \mathbf{H}_1 & \mathbf{0} & \ldots & \mathbf{0} \\ \mathbf{0} & \mathbf{H}_2 & \ldots & \mathbf{0} \\ \vdots & \vdots & \ldots & \vdots \\ \mathbf{0} & \mathbf{0} & \ldots & \mathbf{H}_{N_t} \end{bmatrix} \tag{5}$$

When MIMO channels are invariant over each FDFR block, that is $\mathbf{H}_l = \mathbf{H}, l = 1, \ldots N_t$, the resulting 'FDFR-block-fading' channel matrix can be written in a simple form as $\mathcal{H} = \mathbf{I}_{N_t} \otimes \mathbf{H}$ with $\mathbf{I}_{N_t}$ denoting the $N_t \times N_t$ identity matrix.

Let $\mathbf{y}_l$ denote the lth $N_r \times 1$ received vector, $\mathbf{y} := [\mathbf{y}_1^T, \ldots, \mathbf{y}_{N_r}^T]^T$, $\mathbf{n}_l$ denote the kth $N_r \times 1$ noise vector and $\mathbf{n} := [\mathbf{n}_1^T, \ldots, \mathbf{n}_{N_r}^T]^T$. The input-output relationship is then [17]:

$$\mathbf{y} = \mathcal{H}\boldsymbol{\Phi}\mathbf{s} + \mathbf{n} = \mathbf{H}_{\text{eq}}\mathbf{s} + \mathbf{n} \tag{6}$$

where the equivalent channel matrix for the entire FDFR block is $\mathbf{H}_{\text{eq}} = \mathcal{H}\boldsymbol{\Phi}$.

2.2. The Receiver With Turbo Decoding

At the receiver end, turbo decoding is carried out to achieve an overall near-ML performance. Two modules, indexed by subscripts $_1$ and $_2$, perform soft decoding of the FDFR-MIMO and ECC parts respectively (see Figure 1). Extrinsic information about $\mathbf{c}$, denoted as $\boldsymbol{\lambda}_E$, from one decoding module is (de-)interleavered to yield *a priori* information about $\mathbf{c}$, denoted as $\boldsymbol{\lambda}_A$, for the other module. After a certain number of iterations or after a certain BER is achieved, a hard decision $\hat{\mathbf{b}}$ is obtained based on the *a posteriori* information about $\mathbf{b}$, denoted as $\boldsymbol{\lambda}_{D2}$, from the ECC decoding module.

Inside each module, the optimal maximum *a posteriori* (MAP) decoder, whether it operates over the GF or over the real/complex field (RCF), requires complexity that increases exponentially with the problem size in general (e.g. the memory length for CC or the block size and the constellation size for RCF code). Several near-optimal algorithms with polynomial complexity have been developed for decoding GF and RCF codes respectively. Those for decoding over GF are well documented when CC or TC is used. We adopt the so-called log-MAP algorithm to decode CC and TC in Reference [22]. To decode RCF coded transmissions over FDFR-MIMO channels, hard sphere decoding (HD-SD) [23–25] and semi-definite programming (SDP) [26] offer two well-known near-ML schemes to generate hard decisions. Other sub-optimal decoding schemes with lower complexity

include zero-forcing (ZF), minimum mean-square error (MMSE) and nulling-cancelling (NC) alternatives [27]. Compared with hard decoding, the soft decoding problem for the real/complex block model has been looked upon only recently. A soft version SD, known as list SD (LSD) [28] was recently proposed to perform soft MIMO channel decoding and was shown to enable MIMO capacity approaching performance. A soft version SDP has also been developed to this end [29]. Recent soft-to-hard SD (SHD-SD) transformation schemes [20,21] achieve comparable performance as LSD at reduced complexity. In this paper, we will use the near-optimal SHD-SD scheme 1 of Reference [20] to decode QPSK modulated FDFR transmissions. Since SHD-SD schemes only work for binary constellations, we will not consider other constellations in this paper.

We now briefly explain the FDFR-MIMO decoding process with SHD-SD schemes. First, by separating the real and imaginary parts of the matrices and vectors in Equation (6), we obtain a real equivalent model as

$$\tilde{\mathbf{y}} = \begin{bmatrix} \mathbf{y}_r \\ \mathbf{y}_i \end{bmatrix} = \begin{bmatrix} \mathbf{H}_{\mathrm{eq},r} & -\mathbf{H}_{\mathrm{eq},i} \\ \mathbf{H}_{\mathrm{eq},i} & \mathbf{H}_{\mathrm{eq},r} \end{bmatrix} \begin{bmatrix} \mathbf{s}_r \\ \mathbf{s}_i \end{bmatrix} + \begin{bmatrix} \mathbf{n}_r \\ \mathbf{n}_i \end{bmatrix} = \tilde{\mathbf{H}}\tilde{\mathbf{s}} + \tilde{\mathbf{n}} \tag{7}$$

Each entry of $\tilde{\mathbf{s}}$, $\tilde{s}_k$ ($k = 1, \ldots, 2N_t^2$), is equal to either $+1$ or -1. Define the *a priori* information, the *a posteriori* information given $\tilde{\mathbf{y}}$, and the extrinsic information of $\tilde{s}_k$ respectively as:

$$\begin{aligned} \lambda_A(\tilde{s}_k) &:= \ln \frac{P(\tilde{s}_k = +1)}{P(\tilde{s}_k = -1)}, \\ \lambda_D(\tilde{s}_k|\tilde{\mathbf{y}}) &:= \ln \frac{P(\tilde{s}_k = +1|\tilde{\mathbf{y}})}{P(\tilde{s}_k = -1|\tilde{\mathbf{y}})}, \\ \lambda_E(\tilde{s}_k|\tilde{\mathbf{y}}) &:= \lambda_D(\tilde{s}_k|\tilde{\mathbf{y}}) - \lambda_A(\tilde{s}_k) \end{aligned}$$

Let $\boldsymbol{\lambda}_A := [\lambda_A(\tilde{s}_1), \ldots, \lambda_A(\tilde{s}_{2N_t^2})]^T$ denote the *a priori* vector of $\tilde{\mathbf{s}}$. With the AWGN assumption and the max-log approximation [22], we can approximate the extrinsic information of $\tilde{s}_k$ as [21,28]:

$$\begin{aligned} \lambda_E(\tilde{s}_k|\tilde{\mathbf{y}}) = \frac{1}{2}\max_{\mathbf{x}\in\mathbb{X}_{k,+1}} \left\{ -\frac{1}{\sigma^2}||\tilde{\mathbf{y}} - \tilde{\mathbf{H}}\mathbf{x}||^2 + \mathbf{x}^T\boldsymbol{\lambda}_A \right\} \\ - \frac{1}{2}\max_{\mathbf{x}\in\mathbb{X}_{k,-1}} \left\{ -\frac{1}{\sigma^2}||\tilde{\mathbf{y}} - \tilde{\mathbf{H}}\mathbf{x}||^2 + \mathbf{x}^T\boldsymbol{\lambda}_A \right\} - \lambda_A(\tilde{s}_k) \end{aligned}$$

where $\mathbf{x}$ is the candidate of $\tilde{\mathbf{s}}$, $\mathbb{X}_{k,+1} := \{\mathbf{x}|x_k = +1\}$ and $\mathbb{X}_{k,-1} := \{\mathbf{x}|x_k = -1\}$.

Relying on the spatially independent channel assumption, $\tilde{\mathbf{H}}$ has full column rank almost surely. Therefore, we can find a vector $\mathbf{y}_A$ satisfying

$$2\tilde{\mathbf{H}}^T\mathbf{y}_A = \sigma^2\boldsymbol{\lambda}_A \tag{8}$$

Using Equation (8), we can rewrite the extrinsic information of $\tilde{s}_k$ as:

$$\begin{aligned} \lambda_E(\tilde{s}_k|\tilde{\mathbf{y}}) = -\frac{1}{2\sigma^2}\min_{\mathbf{x}\in\mathbb{X}_{k,+1}} ||\tilde{\mathbf{y}} + \mathbf{y}_A - \tilde{\mathbf{H}}\mathbf{x}||^2 \\ + \frac{1}{2\sigma^2}\min_{\mathbf{x}\in\mathbb{X}_{k,-1}} ||\tilde{\mathbf{y}} + \mathbf{y}_A - \tilde{\mathbf{H}}\mathbf{x}||^2 - \lambda_A(\tilde{s}_k) \end{aligned} \tag{9}$$

Let $\mathbb{X}$ denote the union of $\mathbb{X}_{k,-1}$ and $\mathbb{X}_{k,+1}$. If $\hat{\mathbf{s}}_{\mathrm{map}} := \arg\min_{\mathbf{x}\in\mathbb{X}} ||\tilde{\mathbf{y}} + \mathbf{y}_A - \tilde{H}\mathbf{x}||^2$, and $\hat{\mathbf{s}}_k := \arg\min_{\mathbf{x}\in\mathbb{X}_{k,-\hat{s}_{k,\mathrm{map}}}} ||\tilde{\mathbf{y}} + \mathbf{y}_A - \tilde{\mathbf{H}}\mathbf{x}||^2$ for $k = 1, \ldots, 2N_t^2$, then Equation (9) can be further simplified as

$$\begin{aligned} \lambda_E(\tilde{s}_k|\tilde{\mathbf{y}}) = -\frac{\hat{s}_{k,\mathrm{map}}}{2\sigma^2}||\tilde{\mathbf{y}} + \mathbf{y}_A - \tilde{\mathbf{H}}\hat{\mathbf{s}}_{\mathrm{map}}||^2 \\ + \frac{\hat{s}_{k,\mathrm{map}}}{2\sigma^2}||\tilde{\mathbf{y}} + \mathbf{y}_A - \tilde{\mathbf{H}}\hat{\mathbf{s}}_k||^2 - \lambda_A(\tilde{s}_k) \end{aligned} \tag{10}$$

Hard sphere decoding (SD) can be used to find $\hat{\mathbf{s}}_{\mathrm{map}}$ and $\{\hat{\mathbf{s}}_k\}_{k=1}^{2N_t^2}$. The soft max-MAP decoding problem is thus converted to a set of hard SD problems. Based on this max-MAP decoder, so termed SHD-SD Scheme 1 in Reference [20], additional approximate schemes have been developed in Reference [20] to trade-off error performance with complexity.

3. Performance Analysis

In this section, we will analyze the error performance of coded FDFR, and show it is capable of enabling a multiplicative diversity effect; namely that the diversity order of coded FDFR is the product of that enabled by ECC and by FDFR respectively. We will also compare the two ECC structures: single-stream CC versus multi-stream CC. The comparison will suggest a single-stream structure that we will further test with simulations presented in the next section.

3.1. Diversity Order

We here resort to a pairwise error probability (PEP) approach to analyze the performance of coded FDFR. Let us assume for now that the MIMO channel remains constant over an entire FDFR block but is

allowed to vary independently from block to block. Consider two different information bit frames $\mathbf{b}^{\langle 1\rangle}$ and $\mathbf{b}^{\langle 2\rangle}$, each with length K_c. They yield two codewords $\mathbf{c}^{\langle 1\rangle}$ and $\mathbf{c}^{\langle 2\rangle}$ with length N_c after ECC, with either a single-stream or a multi-stream structure. These two codewords differ from each other in d positions and so do the interleaved codewords. Although, it is possible that these d positions could be in close proximity for a certain interleaver and a certain pair of codewords, considering the fact that the interleaver $\mathbf{\Pi}$ is random with a different realization per frame, these d positions will most likely be sufficiently far apart provided that the interleaver size is sufficiently long. Under this assumption, we can henceforth consider that after constellation mapping, the two symbol sequences $\mathbf{f}^{\langle 1\rangle}$ and $\mathbf{f}^{\langle 2\rangle}$ still have d different symbols, and in any FDFR block the vectors $\mathbf{s}(k)^{\langle 1\rangle}$ and $\mathbf{s}(k)^{\langle 2\rangle}$ differ in at most one symbol, where $k \in [1, K]$ indexes the FDFR block and K is the number of FDFR blocks.

After LCF coding, LST mapping and propagation through the channel $\mathbf{H}(k)$, the equivalent channel matrix for the kth FDFR block is $\mathbf{H}_{\text{eq}}(k)$. The resulting symbol vectors are $\{\mathbf{z}(k)^{\langle 1\rangle} = \mathbf{H}_{\text{eq}}(k)\mathbf{s}(k)^{\langle 1\rangle}\}_{k=1}^{K}$ and $\{\mathbf{z}(k)^{\langle 2\rangle} = \mathbf{H}_{\text{eq}}(k)\mathbf{s}(k)^{\langle 2\rangle}\}_{k=1}^{K}$. Out of K blocks, only d of them are different. Without causing confusion, we will use $\{\mathbf{z}(i)^{\langle 1\rangle}\}_{i=1}^{d}$ and $\{\mathbf{z}(i)^{\langle 2\rangle}\}_{i=1}^{d}$ to denote them. When $\mathbf{s}(i)^{\langle 1\rangle}$ and $\mathbf{s}(i)^{\langle 2\rangle}$ are different in the mth symbol, the Euclidean distance between $\mathbf{z}(i)^{\langle 1\rangle}$ and $\mathbf{z}(i)^{\langle 2\rangle}$ is:

$$||\mathbf{z}(i)^{\langle 1\rangle} - \mathbf{z}(i)^{\langle 2\rangle}||^2 = ||\mathbf{h}_{eq,m}(i)||^2 |\Delta s_m(i)|^2 \quad (11)$$

where $\mathbf{h}_{\text{eq},m}(i)$ is the mth column of the equivalent channel matrix $\mathbf{H}_{\text{eq}}(i)$, and $|\Delta s_m(i)|^2$ is the Euclidean distance between the two different symbols $s_m(i)^{\langle 1\rangle}$ and $s_m(i)^{\langle 2\rangle}$. With δ^2 standing for the minimum Euclidean distance between two symbols, we have that

$$|\Delta s_m(i)|^2 \geq \delta^2 \quad (12)$$

Since $\mathbf{H}_{\text{eq}} = \mathcal{H}\mathbf{\Phi}$, by the definitions of $\mathcal{H}$ in Equation (5) and $\mathbf{\Phi}$ in Equation (4), if the mth symbol is in the gth FDFR sub-block, we then have

$$\begin{aligned} ||\mathbf{h}_{\text{eq},m}(i)||^2 = ||\mathcal{H}(i)\phi_m||^2 &= \sum_{l=1}^{N_\text{r}} \sum_{j=1}^{N_\text{t}} |h_{l,j}(i)|^2 |\theta_{g,(j,m)}|^2 \\ &= \frac{1}{N_\text{t}} \sum_{l=1}^{N_\text{r}} \sum_{j=1}^{N_\text{t}} |h_{l,j}(i)|^2 \end{aligned} \quad (13)$$

where ϕ_m is the mth column of $\mathbf{\Phi}$, $\theta_{g,(j,m)}$ is the (j, mN_t)th entry of $\mathbf{\Theta}_g$, $h_{l,j}(i)$ is the (l,j)th entry of $N_\text{r} \times N_\text{t}$ channel matrix $\mathbf{H}(i)$ and $\mathcal{H}(i) = \mathbf{I}_{N_\text{t}} \otimes \mathbf{H}(i)$. Equation (13) is true because all entries of $\mathbf{\Theta}_g$ have equal norm $1/\sqrt{N_t}$.

From Equation (11), (12) and (13), the overall Euclidean distance of these two sequences obeys

$$\begin{aligned} d_{1,2}^2 &= \sum_{i=1}^{d} ||\mathbf{z}^{\langle 1\rangle}(i) - \mathbf{z}^{\langle 2\rangle}(i)||^2 \\ &\geq \frac{\delta^2}{N_\text{t}} \sum_{i=1}^{d} \sum_{l=1}^{N_\text{r}} \sum_{j=1}^{N_\text{t}} |h_{l,j}(i)|^2 \end{aligned} \quad (14)$$

The PEP for a given channel realization, $P_{1,2|\{H\}} := P(\mathbf{c}^{\langle 1\rangle} \to \mathbf{c}^{\langle 2\rangle} | \{\mathbf{H}(k)\})$, can be upper bounded as:

$$P_{1,2|\{H\}} \leq Q\left(\sqrt{\frac{\delta^2/N_\text{t} \sum_{i=1}^{d} \sum_{l=1}^{N_\text{r}} \sum_{j=1}^{N_\text{t}} |h_{l,j}(i)|^2}{2N_0}} \right)$$

where $Q(x) := (1/\sqrt{2\pi}) \int_x^\infty exp(-\alpha^2/2) d\alpha$. Using the Chernoff bound $Q(x) \leq (1/2)\exp(-x^2/2)$ and averaging over all h's, we obtain the average PEP as:

$$P_{1,2} \leq \frac{1}{2} \left[\int \exp\left(-\frac{\delta^2}{4N_\text{t}N_0} \alpha^2/2 \right) f(\alpha) d\alpha \right]^{dN_\text{t}N_\text{r}}$$

where $f(\alpha)$ is the probability density function (PDF) of the channel amplitude $\alpha = |h_{l,j}|$ between each transmit/receive antenna pair (l,j), which is assumed to be spatially independent and identically distributed (i.i.d.). In the case of Rayleigh fading, the average PEP is obtained as:

$$P_{1,2} \leq \frac{1}{2} \left(1 + \frac{\delta^2}{4N_\text{t}N_0} \right)^{-dN_\text{t}N_\text{r}} \quad (15)$$

Equation (15) shows that the PEP exhibits diversity order $dN_\text{t}N_\text{r}$. After applying the union bound to all error events, we can upper-bound the average BER of coded FDFR as [30]

$$P_b^F \leq \frac{1}{2} \sum_{d=d_{\min}}^{N_c} B_d \left(1 + \frac{\delta^2}{4N_\text{t}N_0} \right)^{-dN_\text{t}N_\text{r}} \quad (16)$$

where $d_{\min}$ is the minimum Hamming distance of the block ECC, or the free distance of the CC, and B_d is

the average number of bit errors associated with error events of distance d. By definition, we have

$$B_d = \sum_{w=1}^{K_c} \frac{w}{K_c} A_{w,d} \tag{17}$$

where $A_{w,d}$ denotes the number of error events with input sequence weight w and output sequence weight d, and K_c is the number of information bits per input frame (cf. Subsection 2.1). Equation (16) shows that a maximum diversity order $d_{\min}N_tN_r$ is possible with coded FDFR.

Although we assume that MIMO channels remain constant over an FDFR block, this is not necessary. When MIMO channels are both spatially and temporally independent, with slight modifications, it can be easily shown that the diversity order $d_{\min}N_tN_r$ still holds for coded FDFR. In the case of temporally correlated time-varying MIMO channels, a second interleaver $\mathbf{\Pi}^{(2)}$ must be appended after the FDFR module and before transmission to decorrelate the MIMO channels. If the channels change fast enough or the frame size is large enough, then the equivalent channels can still be treated as independent. However, if the channels change very slowly, the full diversity provided by channels is less than $d_{\min}N_tN_r$. In the extreme case when the MIMO channels remain invariant over the entire frame but vary independently from frame to frame, the overall diversity order is only that enabled by the FDFR space-time codes; namely N_tN_r for uncoded FDFR. No extra diversity is gained with ECC. This is because Equation (14) now becomes

$$d_{1,2}^2 = \sum_{i=1}^{d} ||\mathbf{z}^{\langle 1\rangle}(i) - \mathbf{z}^{\langle 2\rangle}(i)||^2 \geq \frac{d\delta^2}{N_t} \sum_{l=1}^{N_r} \sum_{j=1}^{N_t} |h_{l,j}(i)|^2 \tag{18}$$

The average BER of coded FDFR over Rayleigh frame-fading channels is thus

$$\begin{aligned} P_b^F &\leq \frac{1}{2} \sum_{d=d_{\min}}^{N_c} B_d \left(1 + \frac{d\delta^2}{4N_tN_0}\right)^{-N_tN_r} \\ &\leq \frac{1}{2} \left(1 + \frac{d_{\min}\delta^2}{4N_tN_0}\right)^{-N_tN_r} \sum_{d=d_{\min}}^{N_c} B_d \end{aligned} \tag{19}$$

Clearly, the diversity order is N_tN_r, which is the diversity enabled by uncoded FDFR [17]. Different choices of ECC will affect B_d in Equation (16) and therefore ECC will enhance error performance only through the coding gain. When the MIMO channels are block-fading with L independent realizations per frame, then the diversity order of coded FDFR is at most $\min(L, d_{\min})N_tN_r$. Note that the term 'block' in 'block-fading' refers to the channel coherence time.

3.2. Multi-Stream CC versus Single-Stream CC

We now consider the structure of the ECC module and delineate trade-offs between the single-stream ECC of Figure 2 and the multi-stream ECC of Figure 3(a). In general, it is hard to establish analytically which encoding structure is better. As it will be shown later in next section, our coded FDFR offers good performance improvement over coded V-BLAST only when weak codes are used. For this reason, we will focus on the special case of multi-stream terminated-CC versus single-stream terminated-CC.

When the same CC generating function is used, the free distances of single-stream and multi-stream structures are identical. It follows from Equation (16) that BER performance depends on $\{B_d\}_{d=d_{\min}}^{N_c}$. For simplicity, let us consider that: (i) the overall length of the output sequence is N_c for both structures; (ii) there are only two sub-streams in the multi-stream structure and (iii) the same CC generator with memory m and rate R_c is used per encoder. Then the single-stream structure has input sequences with length $N_cR_c - m$ and the encoding process is terminated at the stage $N_cR_c - m$. Each sub-encoder in the two-stream structure has input sequences with length $N_cR_c/2 - m$ and the encoding process is terminated at the stage $N_cR_c/2 - m$. Without loss of generality, the two-stream structure is equivalent to the single-stream structure with m zeros inserted between the $(N_cR_c/2 - m)$th bit and the $(N_cR_c/2 - m + 1)$st bit, as depicted in Figure 4.

We now compare B_d^s and B_d^2 for the single-stream and the two-stream structures respectively. Since the two structures use the same trellis, for any given d and w, all error events with input sequence weight w and output sequence weight d that are counted in $A_{w,d}^2$ for the two-stream structure will also be counted in $A_{w,d}^s$ for the single-stream structure. However, $A_{w,d}^s$ also includes those error events with one or more out of w non-zero bits falling between $N_cR_c/2 - m$ and

Fig. 4. The equivalent single-stream CC model of the multi-stream CC.

$N_c R_c/2$. For the two-stream structure, those error events will never happen, since zeros have been inserted at those positions. Therefore, we have $A^s_{w,d} \geq A^2_{w,d}$ for any w and d, which implies that $B^s_d \geq B^2_d$ according to Equation (17). Hence, the two-stream CC structure offers better BER performance than the single-stream CC one. This conclusion is reasonable because in the two-stream structure, the m zeros in the middle of the input sequence are known. In the Viterbi decoding process, these known zeros help paths converge in the trellis. If the BER of the two-stream CC is P_b, then the BER for the single-stream CC can be roughly approximated as $(1 + m/(N_c R_c - m))P_b$. It should be pointed out that by inserting m zeros, the two-stream CC sacrifices data rate. When R_c is fixed, for large N_c, both the rate loss of the two-stream CC and the error performance loss of the single-stream CC are negligible. Therefore, the two are expected to exhibit comparable performance. This argument for the 2-stream CC can be easily extended to a general multi-stream CC. Therefore, the multi-stream and the single-stream CC have no big difference when the frame length is large. The reason behind this is because CC is a highly-structured ECC. Things could be different when a further randomized ECC, such as LDPC or turbo codes, is used. Quantitative comparison between the multi-stream and single-stream structures for LDPC and TC is interesting but will not be pursued in this paper.

3.3. Comparison With Coded V-BLAST

Since V-BLAST is the simplest LST code achieving full rate and coded V-BLAST has been shown to be capacity approaching [21,28], which means it is asymptotically optimal, we will use coded V-BLAST as a benchmark. The latter can be obtained by simply replacing the FDFR design module in Figure 1 with a serial to parallel converter. Both coded FDFR and coded V-BLAST have the same transfer rate $R_c N_t \log_2 M$ bits per channel use, for a given ECC rate R_c and constellation size M. When fading channels are both spatially and temporally i.i.d., the average BER for coded V-BLAST can be similarly upper-bounded by:

$$P_b^V \leq \sum_{d=d_{\min}}^{N_c} \frac{B_d}{2} \left(1 + \frac{\delta^2}{4N_0}\right)^{-dN_r} \tag{20}$$

The diversity order of coded V-BLAST is thus $d_{\min} N_r$; i.e. $1/N_t$ that of coded FDFR. To achieve identical BER performance, let the SNR needed for coded V-BLAST be $\gamma_v = \delta_v^2/(2N_0)$ and the SNR needed for coded FDFR $\gamma_f = \delta_f^2/(2N_0)$. Comparing Equation (15) with Equation (20), it follows that the SNR gain of coded FDFR over coded V-BLAST is approximately

$$G := \frac{\gamma_v}{\gamma_f} = \frac{\gamma_v}{2N_t[(1+\gamma_v/2)^{1/N_t} - 1]} \overset{N_t \to \infty}{\longrightarrow} \frac{\gamma_v/2}{\ln(1+\gamma_v/2)} \tag{21}$$

Equation (21) is very similar to the gain that ECC with unitary precoding (ECC-UP) offers over ECC without precoding (ECC-only) with N_t viewed as the LCF size M in Reference [31]. This similarity is quite reasonable, since from Equation (13) we deduce that the diversity factor N_t relies on an LCF encoder with size N_t. From Equation (21), we also infer that increasing N_t will increase the diversity gain. However, this gain increment decreases as N_t increases. Considering the complexity increment as N_t increases, FDFR is more useful when N_t is small, for example $N_t = 2$. When MIMO channels are frame-fading, it is easy to see from Equation (19) that in order to achieve the same BER performance, the SNR gain that coded FDFR enjoys over coded V-BLAST is now

$$G := \frac{\gamma_v}{\gamma_f} = \frac{d_{\min}\gamma_v}{2N_t[(1+d_{\min}\gamma_v/2)^{1/N_t} - 1]} \overset{N_t \to \infty}{\longrightarrow} \frac{d_{\min}\gamma_v/2}{\ln(1+d_{\min}\gamma_v/2)} \tag{22}$$

Comparing Equation (21) with Equation (22), we notice that for a given γ_v, coded FDFR exhibits larger gain over coded V-BLAST in frame-fading rather than fast fading channels. However, the union bound analysis implies that this is valid only at high SNR, i.e. $\gamma \geq \gamma_{\text{th}}$, where γ_{th} is the minimum SNR needed to achieve a certain BER, for example $P_b = 10^{-4}$. Since the diversity order over frame-fading channels is $d_{\min}$ times less than that over i.i.d. channels, we expect that γ_{th} over frame-fading channels is larger than that over i.i.d. channels. We will corroborate this later on with simulations.

4. Simulations

We carry out simulations with different ECCs for QPSK modulated MIMO transmissions to compare BER of coded V-BLAST and FDFR systems. Except

for Simulation 4, both systems use the single-stream ECC structure. We use the SHD-SD scheme 1 for both systems in Reference [20]. The interleaver size is chosen to be 2^{10}. Apart from Simulation 3, the spatially i.i.d. channels remain invariant on a per FDFR block basis but change independently from FDFR block to block. In each figure, curves with the same marker correspond to BER for the same system (either coded V-BLAST or coded FDFR) at different iterations.

Notice that the equivalent channel matrix $\mathbf{H}_{\text{eq}}$ in Equation (6) is an $N_{\text{t}}^2 \times N_{\text{r}}^2$ complex matrix, which implies a considerable increase in decoding complexity relative to V-BLAST with block size N_{t} for the same antenna setup.

4.1. Simulation 1

Figures 5 and 6 depict BER performance comparisons between coded V-BLAST and coded FDFR, when relatively weak codes (CC and high rate TC) are used as ECC in a 2×2 antenna setup. BER curves with three iterations are shown in Figure 5. We observe that with rate 1/2 CC the performance gain after the 2nd iteration is negligible. The same behavior has been observed with rate 3/4 TC during the simulation process, although the BER curve of the 3rd iteration is not shown in Figure 6. Therefore, we will only show BER curves of two iterations for these codes in the rest of this paper. We use rate 1/2 CC with memory 2, feedback polynomial $G_{\text{r}}(D) = 1 + D + D^2$, and feedforward polynomial $G(D) = 1 + D^2$. About 1.5 dB gain at BER $= 10^{-4}$ is offered by the FDFR design when CC is used. We also use rate 3/4 parallel concatenated convolutional codes (PCCC) in Figure 6, composed of two CC modules parameterized as before. The puncturing pattern used retains all systematic bits and takes one bit every 6 bits from each coded stream. Five iterations are performed inside the decoding module for rate 3/4 turbo codes. Two outer iterations are performed between the two decoding modules. Figure 6 shows the BER comparison for rate 3/4 turbo codes in a 2×2 setup. In this case, coded FDFR outperforms coded V-BLAST by about 2 dB.

4.2. Simulation 2

In this simulation, we use a rate 1/2 PCCC constructed as the rate $3/4$ PCCC except for the puncturing pattern. Here we keep all the systematic bits and every other bit from each coded stream. Figure 7 depicts the comparison in a 2×2 setup with three outer iterations. Five iterations are performed inside the decoding module for rate 1/2 TC. We see no performance improvement with FDFR, which is reasonable when such a strong code is used with $N_{\text{r}} = N_{\text{t}}$. Thanks to the larger diversity order, uncoded FDFR outperforms uncoded V-BLAST at high SNR noticeably [17].

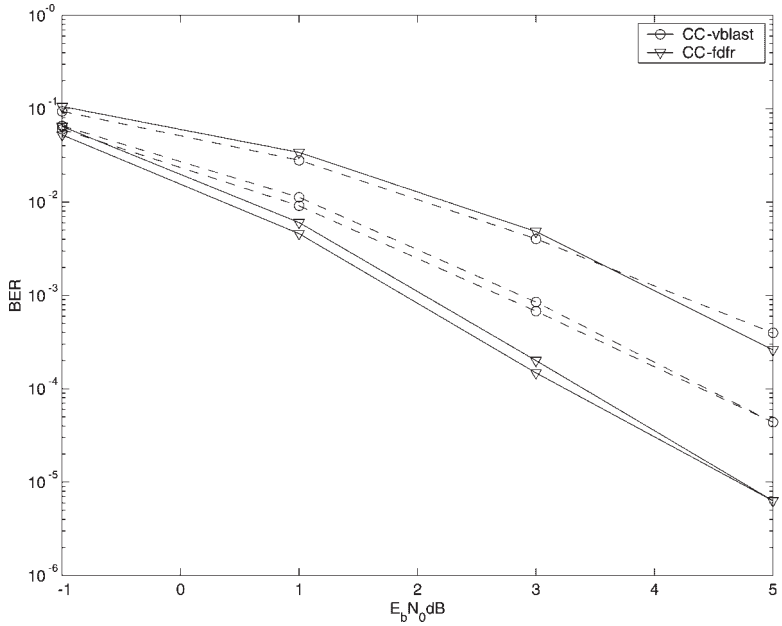

Fig. 5. 1/2 CC with FDFR vs. 1/2 CC with V-BLAST in a 2×2 setup.

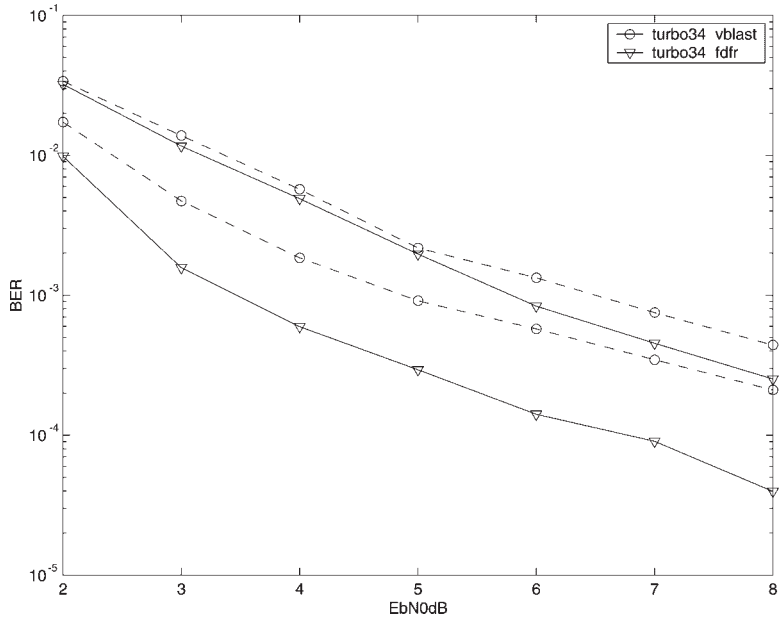

Fig. 6. 3/4 turbo codes with FDFR versus 3/4 turbo codes with V-BLAST in a 2×2 setup.

However, when we use strong codes such as rate 1/2 TC, the diversity gains are already high at low SNR (i.e. the slope of the BER curve is already very steep). In this case, the larger diversity order enabled by FDFR brings no advantage.

Figure 8 shows the same comparison in a 2×5 setup. By increasing N_r, both coded FDFR and coded V-BLAST benefit from the extra energy collected and the extra diversity provided by N_r receive antennas. But the turbo gain between iterations becomes smaller. We further observe that in the 2×5 case, even the coded LST system with rate 1/2 TC can benefit from the FDFR design by about 0.5 dB over the coded V-BLAST system.

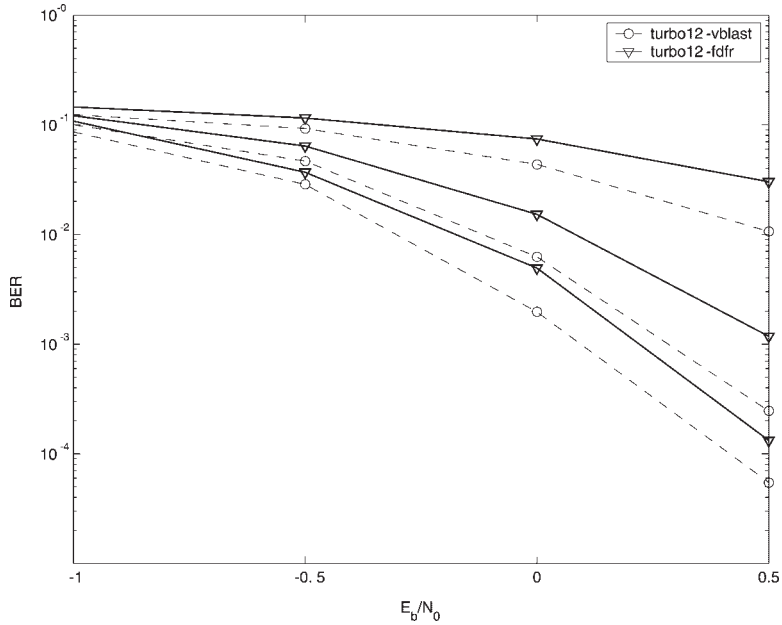

Fig. 7. 1/2 turbo codes with FDFR versus 1/2 turbo codes with V-BLAST in a 2×2 setup.

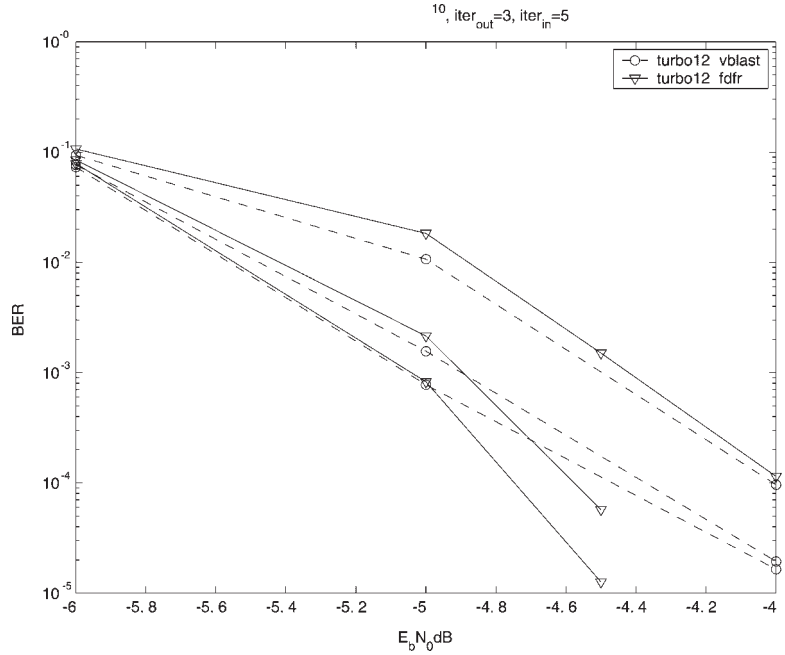

Fig. 8. 1/2 turbo codes with FDFR versus 1/2 turbo codes with V-BLAST in a 2×5 setup.

4.3. Simulation 3

We now assume that the MIMO channel is fading on a frame by frame basis; that is, our MIMO channel remains invariant over the entire ECC frame but fades independently across ECC frames. Figure 9 compares coded FDFR with coded V-BLAST in a 2×2 setup, when a rate 1/2 CC is used. Compared with Figure 5 of Simulation 1, the diversity order and the iterative gain decreases for both coded FDFR and coded V-BLAST. Besides, coded FDFR now has about 2 dB gain over coded V-BLAST. Relative to i.i.d. channels, about 6 dB

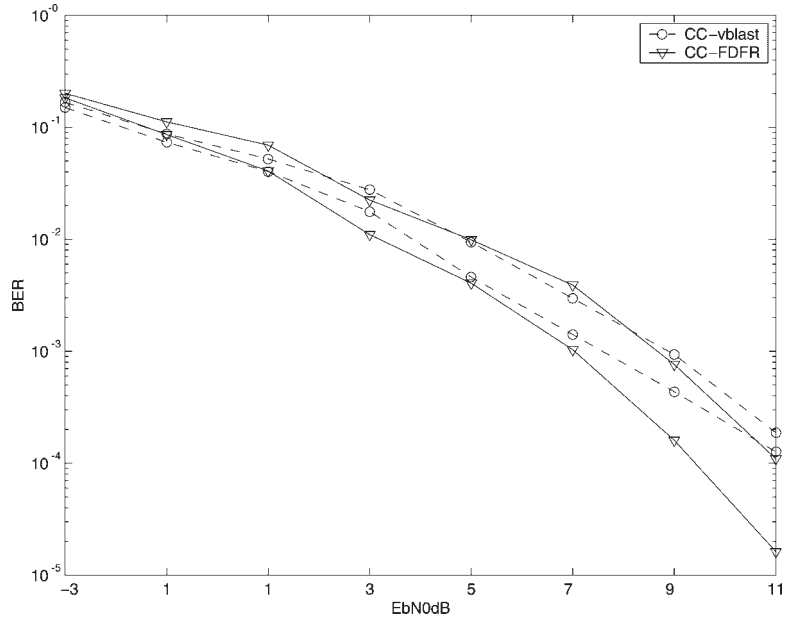

Fig. 9. Bit error rate (BER) performance of 1/2 CC with FDFR versus that of 1/2 CC with V-BLAST in a 2×2 frame-fading setup.

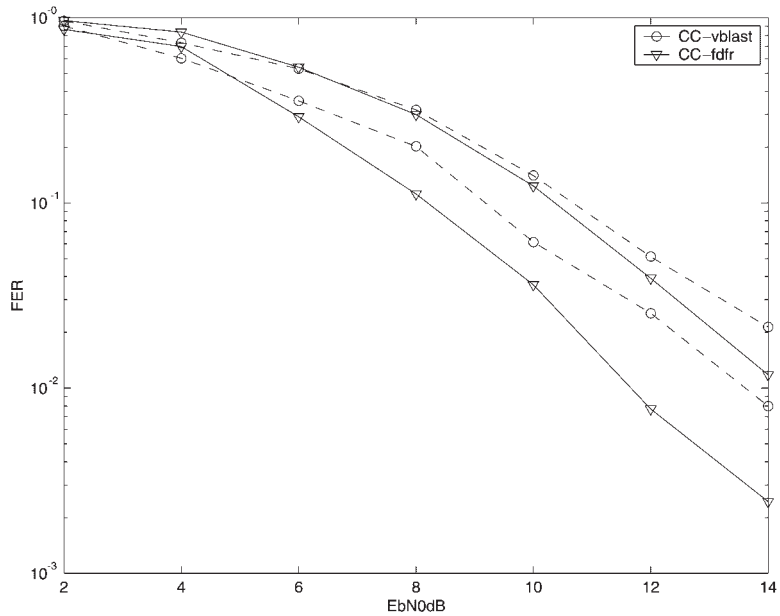

Fig. 10. Frame error rate (FER) performance of 1/2 CC with FDFR versus that of 1/2 CC with V-BLAST in a 2×2 frame-fading setup.

extra SNR is required to achieve BER $= 10^{-4}$ in frame-by-frame-fading channels. This observation matches our analysis in Section 3. The frame error rate (FER) curves of the same simulations are shown in Figure 10.

4.4. Simulation 4

The performance comparison between single-stream versus multi-stream coded structures with CC as an encoder in coded FDFR is depicted in Figure 11. There are two sub-streams in the multi-stream structure. Each sub-stream has input length 2^9. We can see that the two structures exhibit basically identical BER performance.

4.5. Simulation 5

We have used the SHD-SD Scheme 1 of Reference [20] to decode MIMO channels for both FDFR system

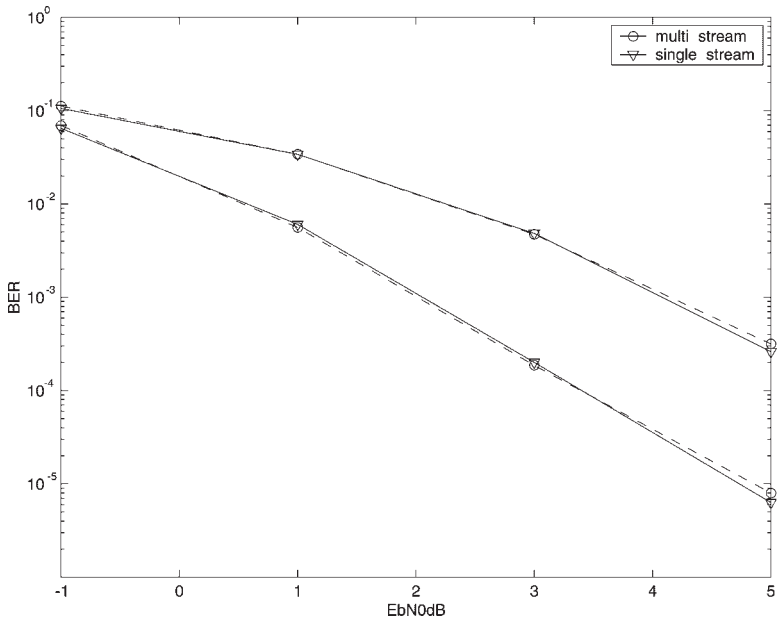

Fig. 11. 1/2 multi-stream CC with FDFR versus 1/2 single-stream CC with FDFR in a 2×2 setup.

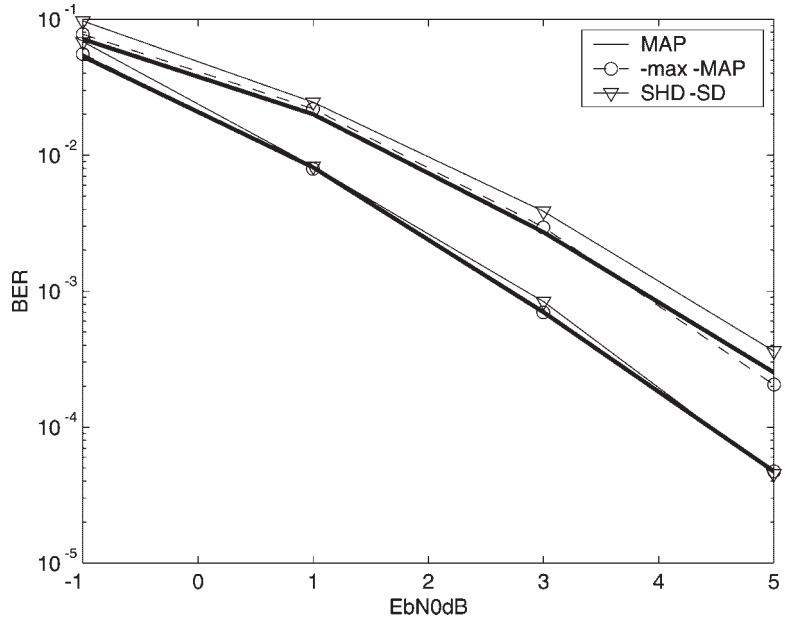

Fig. 12. CC coded V-BLAST with SHD-SD Scheme 1, max-MAP and MAP decoding in a 2×2 setup.

and V-BLAST system. In this simulation, we will measure the performance loss with the max-log approximation. Figure 12 shows the BER curves of convolutional coded V-BLAST system with SHD-SD Scheme 1, brute-force max-MAP decoding, and brute-force-MAP decoding respectively. As we can see, the performance difference between different decoding schemes is negligible, which verifies that our SHD-SD Scheme 1 is near-optimal.

4.6. Simulation 6

It is well known that Alamouti's 2×2 scheme also achieves full diversity with low complexity. Although throughout this paper, we have used coded V-BLAST as our reference, it will be interesting to compare our coded FDFR system with coded Alamouti as well. In a coded Alamouti system after the information bits are ECC coded and interleaved, coded bits are mapped to 16-QAM symbols to achieve the same transmission rate as its coded FDFR counterpart. Those 16-QAM symbols are then transmitted with the Alamouti scheme. Soft brute-force-MAP MIMO-decoding/demapping is used at the receiver. Figure 13 depicts the comparison of CC coded FDFR with CC coded Alamouti in a 2×2 setup. From the figure we can see that coded Alamouti has better performance than coded FDFR in the first iteration. A possible reason for this is that being an orthogonal design, Alamouti's scheme converts the MIMO channels to a set of SISO channels, thereby avoiding interference among different symbols. However, about 1 dB gain is offered by FDFR at the second iteration. Another interesting observation is that there is almost no iterative gain for coded Alamouti, which is consistent with the assertion in Reference [32].

Remark: From Figures 5 to 13, we observe an evident iterative gain for both coded V-BLAST and coded FDFR. This observation is different from the conclusion in Reference [32], where it is claimed that no improvement is brought by performing outer iterations between the space-time decoding module and the decoding module for the outer code. This is because the assertion in Reference [32] has been established only for space-time orthogonal designs, where the equivalent channel is diagonal and thus the *a priori* information from other symbols provides no extra information for the current symbol. This conclusion agrees with Simulation 6, where almost no improvement is brought by increasing the number of outer-iterations between MIMO decoding/demappping and ECC decoding. However, the assertion in Reference [32] clearly does not hold for FDFR and V-BLAST.

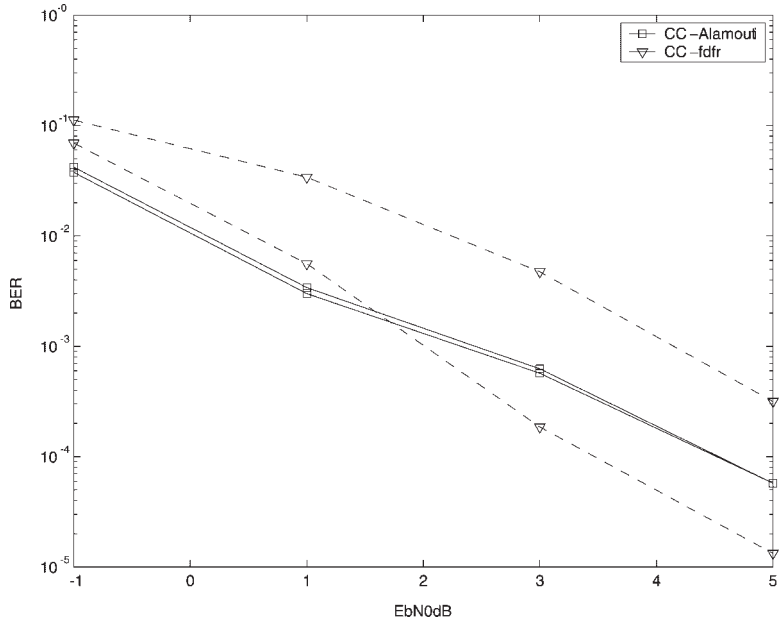

Fig. 13. CC coded FDFR vs. CC coded 16-QAM Alamouti in a 2×2 setup.

5. Conclusions

In this paper, we improved the performance of a coded FDFR multi-antenna system using turbo decoding. For N_t transmit and N_r receive antennas, rate R_c error-control coding and constellation size M, high rate ($R_c N_t \log_2 M$ information bits per channel use) and high diversity order (up to $d_{\min} N_t N_r$) are achieved. Compared with its coded V-BLAST counterpart, coded FDFR improves performance without sacrificing rate when weak ECC is used. The price paid is an increase in complexity. Deriving a soft FDFR decoder with low complexity is an issue worth pursuing in future research.

References

1. Gallager RG. Low density parity check codes. *IRE Transactions on Information Theory* 1962; **IT-8**: 21–28.
2. Mackay DJC, Neal RM. Near Shannon limit performance of low density parity check codes. *Electronics Letters* 1996; **32**(18): 1645–1646.
3. Berrou C, Glavieux A. Near optimum error correcting coding and decoding: turbo-codes. *IEEE Transactions on Communications* 1996; **44**(10): 1261–1271.
4. Viterbi AJ. An intuitive justification and a simplified implementation of the MAP decoder for convolutional codes. *IEEE Journal on Selected Areas in Communications* 1998; **16**(2): 260–264.
5. Boutros J, Viterbo E, Rastello C, Belfiore JC. Good lattice constellations for both Rayleigh fading and Gaussian channels. *IEEE Transactions on Information Theory* 1996; **42**(2): 502–518.
6. Boutros J, Viterbo E. Signal space diversity: a power- and bandwidth-efficient diversity technique for the Rayleigh fading channel. *IEEE Transactions on Information Theory* 1998; **44**(4): 1453–1467.
7. Ma X, Giannakis GB. Complex field coded MIMO systems: performance, rate, and tradeoffs. *Wireless Communications and Mobile Computing* 2002; **2**(7): 693–717.
8. Xin Y, Wang Z, Giannakis GB. Space-time diversity systems based on linear constellation precoding. *IEEE Transactions on Wireless Communications* 2003; **2**(2): 294–309.
9. Wang Z, Giannakis GB. Complex-field coding for OFDM over fading wireless channels. *IEEE Transactions on Information Theory* 2003; **49**(3): 707–720.
10. Telatar IE. Capacity of multi-antenna Gaussian channels. *European Transactions Telecommunications* 1999; **10**(6): 585–595.
11. Alamouti SM. A simple transmit diversity technique for wireless communications. *IEEE Journal on Selected Areas in Communications* 1998; **16**(8): 1451–1458.
12. Tarokh V, Jafarkhani H, Calderbank AR. Space-time block codes from orthogonal designs. *IEEE Transactions on Information Theory* 1999; **45**(5): 1456–1467.
13. Tarokh V, Seshadri N, Calderbank AR. Space-time codes for high data rate wireless communication: performance criterion and code construction. *IEEE Transactions on Information Theory* 1998; **44**(2): 744–765.
14. Foschini GJ. Layered space-time architecture for wireless communication in a fading environment when using multiple antennas. *Bell Laboratories Technical Journal* 1996; **1**(2): 41–59.
15. Wolniansky PW, Foschini GJ, Golden GD, Valenzuela RA. V-BLAST: an architecture for realizing very high data rates over the rich-scattering wireless channel. In *URSI International Symposium on Signals, Systems, and Electronics*, September 1998, pp. 295–300.

16. Heath RW, Jr., Paulraj AJ. Linear dispersion codes for MIMO systems based on frame theory. *IEEE Transactions on Signal Processing* 2002; **50**(10): 2429–2441.
17. Ma X, Giannakis GB. Full-diversity full-rate complex-field space-time coding. *IEEE Transactions on Signal Processing* 2003; **51**(11): 2917–2930.
18. El Gamal H, Damen MO. Universal space-time coding. *IEEE Transactions on Information Theory* 2003; **49**(5): 1097–1119.
19. Wang R, Wang Z, Giannakis GB. Combining Galois with complex field coding for space-time communications. *European Telecommunications Transactions* 2003; **14**(1): 25–36.
20. Wang R, Giannakis GB. Approaching MIMO channel capacity with reduced-complexity soft sphere decoding. In *Proceedings of Wireless Communications and Networking Conference*, Atlanta, GA, March 21–25, 2004, downloadable from http://spincom.ece.umn.edu/conference.html.
21. Wang R, Giannakis GB. Approaching MIMO Channel capacity with reduced-complexity soft sphere decoding. *IEEE Transactions on Communications* 2004 (*revised*).
22. Robertson P, Villebrun E, Hoeher P. A comparison of optimal and suboptimal MAP decoding algorithms operating in the log domain. In *Proceedings of International Conference on Communications*, Seattle, Washington, June 1995, Vol. 2, pp. 1009–1013.
23. Pohst M. On the computation of lattice vectors of minimal length, successive minima and reduced bases with applications. In *ACM SIGSAM*, February 1981, Vol. 15, pp. 37–44.
24. Fincke U, Pohst M. Improved methods for calculating vectors of short length in a lattice, including a complexity analysis. *Mathematical Computation* 1985; **44**: 463–471.
25. Hassibi B, Vikalo H. On the expected complexity of sphere decoding. In *Proceedings of 35th Asilomar Conference on Signals, Systems and Computers*, Pacific Grove, CA, November 2001, Vol. 2, pp. 1051–1055.
26. Ma WK, Davidson TN, Wong KM, Luo ZQ, Ching PC. Quasi-maximum-likelihood multiuser detection using semi-definite relaxation with application to synchronous CDMA. *IEEE Transactions on Signal Processing* 2002; **50**(4): 912–922.
27. Hassibi B. An efficient square-root algorithm for BLAST. In *IEEE International Conference on Acoustics, Speech and Signal Processing*, Istanbul, Turkey, 5–9 June 2000, Vol. 2, pp. II737–II740.
28. Hochwald BM, ten Brink S. Achieving near-capacity on a multiple-antenna channel. *IEEE Transactions on Communications* 2003; **51**(3): 389–399.
29. Steingrimsson B, Luo Z-Q, Wong KM. Soft quasi-maximum-likelihood detection for multiple-antenna wireless channels. *IEEE Transactions on Signal Processing* 2003; **51**(11): 2710–2719.
30. Benedetto S, Biglieri E. *Principles of Digital Transmission with Wireless Applications*. Kluwer Academic/Plenum Publishers, New York, 1999.
31. Wang Z, Zhou S, Giannakis GB. Joint coding-precoding with low-complexity turbo-decoding. *IEEE Transactions on Wireless Communications* 2004; **3**(3): 832–842.
32. Bauch G. Concatenation of space-time block codes and turbo-TCM. In *Proceedings of International Conference on Communications*, Vancouver, Canada, 6–10 June 1999, Vol. 2, pp. 1202–1206.

Authors' Biographies

Renqiu Wang was born in Dalian, China, in 1975. She received her B.S. degree in electrical engineering and information science from the University of Science and Technology of China (USTC), 1998. From 1998 to 2001, she worked for the Shanghai Bell Company, China, on switching networks, third generation mobile communication systems and software design for video communication over IP networks. She is now pursuing a Ph.D. in the Department of Electrical and Computer Engineering at the University of Minnesota. Her research interests are signal processing applications in communications, codes on graphs, space-time processing and coding, turbo decoding algorithms and computer networks.

Xiaoli Ma received his B.S. degree in automatic control from Tsinghua University, Beijing, China, in 1998 and the M.Sc. degree and Ph.D. in electrical engineering from the University of Virginia, Charlottesville, VA, in 1999 and the University of Minnesota, Minneapolis, MN, in 2003 respectively. Since August 2003, she has been an assistant professor with the Department of Electrical and Computer Engineering, Auburn University. Her research interests include transmitter and receiver diversity techniques for wireless fading channels, communications over time- and frequency-selective channels, complex-field and space-time coding, channel estimation and equalization algorithms, carrier frequency synchronization for OFDM systems, and wireless sensor networks.

Georgios B. Giannakis received his diploma in electrical engineering from the National Technical University of Athens, Greece, 1981. From September 1982 to July 1986, he was with the University of Southern California (USC), Los Angeles, where he received his M.Sc. in electrical engineering, in 1983, M.Sc. in mathematics, in 1986, and Ph.D. in electrical engineering, in 1986. After lecturing for 1 year at USC, he joined the University of Virginia in 1987, where he became a professor of electrical engineering in 1997. Since 1999, he has been a professor with the Department of Electrical and Computer Engineering at the University of Minnesota, where he now holds an ADC Chair in Wireless Telecommunications. His general interests span the areas of communications and signal processing, estimation and detection theory, time-series analysis and system identification—subjects on which he has published more than 200 journal papers 350 conference papers and two edited books. Current research focuses on transmitter and receiver diversity techniques for single- and multi-user fading communication channels, complex-field and space-time coding, multicarrier, ultra-wide band wireless communication systems, cross-layer designs and distributed sensor networks. G.B. Giannakis is the (co-)recipient of six paper awards from the IEEE Signal Processing (SP) and Communications Societies (1992, 1998, 2000, 2001, 2003, 2004). He also received the SP Society's Technical Achievement Award in 2000. He served as editor-in-chief for the *IEEE SP Letters*, as associate editor for the *IEEE Transaction on Signal Processing* and the *IEEE SP Letters*, as secretary of the SP Conference Board, as member of the SP Publications Board, as member and vice-chair of the Statistical Signal and Array Processing Technical Committee, as chair of the SP for Communications Technical Committee and as a member of the IEEE Fellows Election Committee. He has also served as a member of the IEEE-SP Society's Board of Governors, the editorial board for the *Proceedings of the IEEE* and the steering committee of the *IEEE Transaction on Wireless Communications*.